ORIGINAL ARTICLE

Electron transport behavior of polymer-derived amorphous silicoboron carbonitrides

Kewei Wang[1,2] | Baisheng Ma[1,2] | Ligong Zhang[3] | Zhenzhong Sun[1,2] | Yiguang Wang[4]

[1]School of Mechanical Engineering, Dongguan University of Technology, Dongguan, Guangdong, P. R. China

[2]Neutron Scattering Technical Engineering Research Center, Dongguan University of Technology, Dongguan, Guangdong, P. R. China

[3]State Key Laboratory of Luminescence and Applications, Changchun Institute of Optics, Fine Mechanics and Physics, Chinese Academy of Sciences, Changchun, Jilin, P. R. China

[4]Institute of Advanced Structure Technology, Beijing Institute of Technology, Beijing, P. R. China

Correspondence
Yiguang Wang, Institute of Advanced Structure Technology, Beijing Institute of Technology, Beijing 100081, P. R. China.
Email: wangyiguang@bit.edu.cn

Abstract

Electron transport behavior of polymer-derived amorphous silicoboron carbonitride (a-SiBCNs) ceramics was studied by measuring DC/AC conductivities and optical absorption as functions of the temperature. Structural information of materials was investigated by combining X-ray diffraction (XRD), nuclear magnetic resonance (NMR), X-ray photoelectron spectroscopy (XPS), Raman spectroscopy, and electron paramagnetic resonance (EPR) techniques. Conductive mechanisms and electronic structure of the materials (eg, hopping mechanism, conduction band, band-tail, and defect energy) were deduced by fitting experimental results to theoretical models. Results revealed that DC/AC conduction of materials followed band-tail hopping mechanism instead of previously assumed variable-range hopping mechanism. Hopping mechanism, associated with overlapped band-tail and defect levels, was likely originated by the presence of certain number of defects and highly disordered structure of materials. The content of donor defects in materials was considered to have great influence on the type of electronic mechanism. These results were discussed in line with microstructural evolution of materials.

KEYWORDS
band gap, electrical properties, silicoboron carbonitride, structure

1 | INTRODUCTION

The synthesis of nonoxide silicon-based ceramics by thermal decomposition of polymeric precursors (ie, polymer-derived ceramics, PDCs) has attracted substantial attention recently. Compared with traditional powder metallurgy-based and polycrystalline ceramics, PDCs possess unique processing characteristics [1,2] and structure.[3–8]

In addition, PDCs has demonstrated unique properties [9–14] and potential applications at high temperatures.[16–20] Especially, owing to their amorphous nature, the structure and properties of PDCs change significantly depending on the pyrolysis temperature. A detailed understanding of these changes is key for exploring further applications and establishing the fundamental sciences of these materials.

A detailed study of the conduction mechanism and behavior of PDCs could help investigate the semiconducting properties of these materials as well as establish structure-property relationships. Previous studies have demonstrated that the conduction mechanism of PDCs is closely associated with the concentration of free carbon phase.[21] For example, PDCs with low free-carbon concentrations showed amorphous semiconducting behavior, with the electrons being transported by a band-tail hopping (BTH) mechanism instead of the assumed variable-range hopping mechanism. While the conduction behavior of PDCs has been widely investigated,[22–26] the different conduction mechanisms within these PDCs have not been well researched. For example, Haluschka et.al reported SiCN followed the three-dimensional variable range hopping (3D VRH) while Wang et.al published the BTH mechanism for SiCN.[23,26] Both of them could not provide more interpretation about this different. To better understand the conduction mechanism of these materials, the electronic structure should be determined firstly. But, the complex microstructure of PDC materials makes it difficult to theoretically determine electronic structures. Wang has recently investigated the evolution of the electronic structure of polymer-derived amorphous silicon carbide with the pyrolysis temperature by combining temperature-dependent conductivity and optical absorption measurements.[27] The variations in the electronic structural parameters were discussed according to the microstructural evolutions of the materials. This study proved that the electronic structures information of PDCs could be obtained and investigated by combining conductivity and optical absorption measurements.

In this paper, we systemically studied the electron transport behavior of polymer-derived amorphous silicoboron carbonitrides (a-SiBCNs) pyrolyzed at different temperatures. The conductive mechanisms and electronic structure of the a-SiBCNs were deduced by fitting the obtained results to theoretical models. We showed that the BTH mechanism was related to a unique electronic structure containing overlapped band-tail and defect levels. We also revealed that the pyrolysis temperature altered the conduction behavior of these materials by changing their optical bandgap, band-tail, and defect level characteristics. The conductive mechanisms and the evolution of the electronic structure of these materials were discussed in terms of their structure.

2 | EXPERIMENTAL PROCEDURE

The a-SiBCN ceramics were prepared by pyrolyzing liquid polyborosilazane (PBSN, Institute of Chemistry, Beijing, China). All the a-SiBCN ceramics were prepared similarly. The as-received precursor was first thermally cross-linked at 350°C for 2 hours under a protective flow of ultrahigh purity nitrogen in a quartz tube furnace (GSL-1100X; MTI KJ GROUP, Hefei, Anhui, China). The resultant solid was ground to fine powder (ca. 1 μm in size) using high-energy ball-milling (QM-3A; Midwest Group, Beijing, China). After sieving, the powder was pressed into disks of 16 mm in diameter and 1 mm in thickness at a uniaxial pressure of 10 MPa, followed by cold isostatic pressing at 200 MPa for 2 minutes (CHUAN-XI, Sichuan, China). The disks were subsequently pyrolyzed at 900°C for 4 hours under a steady flow of N_2 in a quartz tube furnace (GSL-1100X; MTI KJ GROUP). The as-obtained samples were further pyrolyzed at different temperatures ranging from 1100 to 1400°C for 3 hours under a flow of ultrahigh purity N_2 in an alumina tube furnace (GSL-1700X; MTI KJ GROUP). The as-obtained SiBCN materials were amorphous with an average composition of $SiB_{0.09}C_{0.95}N_{0.41}$, regardless the pyrolysis temperature.

The X-ray photoelectron spectroscopy (XPS) was carried out on an AXIS ULTRA (Kratos, Manchester, UK) apparatus with monochromatic Al Kα radiation. The spectra were recorded at room temperature (RT) under high vacuum (10^{-9} Torr). To obtain the internal structure of bulk materials, the testing surface of the sample was first polished away 5 μm, and then etched by Ar+ ions to remove additional 2 μm from the surface before testing. The bind energies were calibrated using O1s peak as a reference. The XPS spectra were curve-fitted using the XPS Peak 4.1 program with a Shirley background subtraction. Raman spectra were obtained on Renishaw in-Via Raman microscope (Renishaw, London, UK) with the 514 nm line of Ar+ laser as the excitation source. The X-band (9.6 GHz) electron paramagnetic resonance (EPR) spectra were recorded on a Bruker EMX-10/12 spectrometer (Bruker Instruments, Billerica, MA), of which the sensibility is S/N > 1500:1. The output power was 12 kW. All measurements were carried out at RT. The solid-state NMR experiments were carried out at 7.05 T (75.47MHz Larmor frequency for 29Si) using a Bruker MSL-400 spectrometer. A 4-mm magic angle spinning (MAS) probe with a sample rotation frequency of 62.5 kHz was used for the measurement.

For the conductivity measurements, the surfaces of the specimens were first polished to 1 μm finish. Silver paste electrodes were then painted on the surfaces. The temperature-dependent electrical conductivity of the samples was then measured in a tube furnace within an ultrahigh purity nitrogen environment. The I-V curve was provided by a

semiconductor parameter analyzer (Agilent 4155C; Agilent Technologies, Inc, Santa Clara, CA) over a temperature range of 50-650°C. The AC conductivity were calculated depend on the complex impedance data using Equation (1), which measured on LCR meter (Agilent 4980A; Agilent Technologies) in the frequency range of 50 Hz to 2 MHz at different temperatures.

$$\sigma' = \left[\frac{Z'}{Z'^2 + Z''^2}\right] \times \frac{T}{A} \qquad (1)$$

where Z' and Z'' are the real and imaginary parts of the complex impedance, respectively; T is the thickness of the samples; A is the effective area of the samples.

The same samples used for conductivity measurements underwent optical absorption measurements. The grinded sample powder was mixed with KBr powder and pressed into a disc of 10 and 0.5 mm in diameter and thickness, respectively. The mixture was tested on a UV-3101 double channel spectrometer (Shimadzu Co., Kyoto, Japan). The absorption spectra of the materials were obtained by subtracting the spectrum of pure KBr powder from the spectrum of the mixture.

3 | RESULTS

The temperature-dependent DC conductivity of the a-SiBCN materials is shown in Figure 1. Conductivity increased by several orders of magnitude with the pyrolysis temperature, in line with previous observations for polymer-derived SiC and SiCN ceramics.[26,27] All samples exhibited semiconducting behavior, with positive temperature coefficients for the electrical conductivity. To obtain useful information on the semiconducting electron transport behavior of these
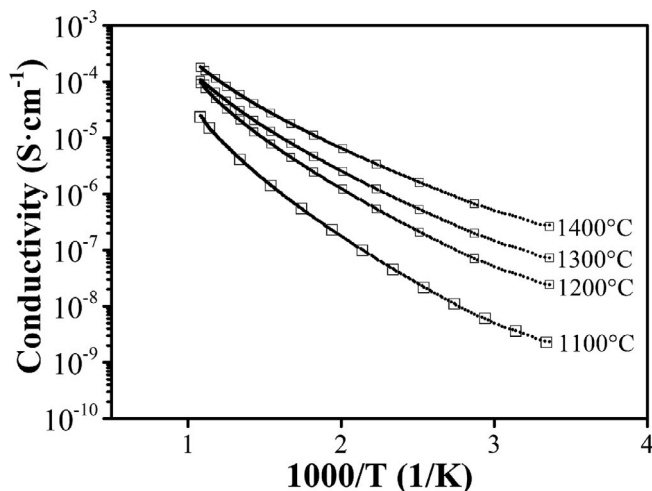
materials, the spectra were fitted to the following theoretical models:

$$\sigma = \sigma_1 e^{-\frac{E_C - E_F}{kT}} + \sigma_2 e^{-\frac{E_A - E_F + w}{kT}} + \sigma_3 e^{-\left(\frac{T_0}{T}\right)^{1/4}} \qquad (2)$$

where E_C, E_A, and E_F are the mobility edge for the conduction band, band-tail, and Fermi levels, respectively; w is the thermal activation energy, which is equal to the phonon energy of the material (we assumed the phonon energy of the a-SiBCN to be in the same range as those of SiC, Si_3N_4, and BN phonons, ca. 135 meV [28–30]); σ_1, σ_2, and σ_3 are the prefactors; and T_0 is the characteristic temperature. The electronic transport contained three different conduction mechanism contributions.[31] The first term in Equation (2) generated by the conduction in extended states, the dominating mechanism at high temperatures. The second term generated by the conduction in band tail states, the dominating mechanism at middle temperatures. The third term derived from the conduction in localized states, the dominating mechanism at low temperatures.

The good fitting obtained between experimental data and the computed parameters of Equation (2) suggested that the conduction of the a-SiBCN ceramics indeed followed an amorphous semiconducting model. The best fitting parameters and square of deviance (χ_1^2) are listed in Table 1.

Figure 2 shows the effect of the frequency on the AC conductivity of a-SiBCN pyrolyzed at 1200°C. The testing temperature is from RT to 300°C. The transition behavior of the conductivity contained two regions. At low frequencies, the conductivity was frequency-independent and remained stable. At high frequencies, the conductivity followed a frequency-dependent Jonscher power law behavior, revealing the existence of a relaxation process.[32–35]

To gain insight into their electronic structure, the optical absorption behavior of the a-SiBCN ceramics was studied. According to theoretical models, the absorption of amorphous semiconductors can be used to determine the direct optical transition gap and the Tauc band-gap within different energy ranges. Over the high energy range, the direct optical transition gap follows the equation [36,37]:

$$(\alpha h v)^2 \infty \left(h v - E_g\right) \qquad (3)$$

where α is the absorption coefficient, hv is the photon energy, and E_g is the optical band gap between conduction band (E_C) and the valence band (E_V). The bandgaps were estimated by the x-intercept slope of dashed line (Figure 3), plotted as $(ahv)^2$ vs hv. The bandgaps for the four samples are listed in Table 2.

Over the low excitation energy range, the Tauc absorption mechanism can be described as follows [38,39]:

$$\alpha h v = B \left(h v - E_T\right)^n \qquad (4)$$

where n is a constant, E_T is the energy gap (ie, Tauc band-gap), and B is a constant. This absorption is associated to

FIGURE 1 Temperature-dependent DC conductivity relationship for amorphous silicoboron carbonitride materials

TABLE 1 Fitting parameters for the conductivity

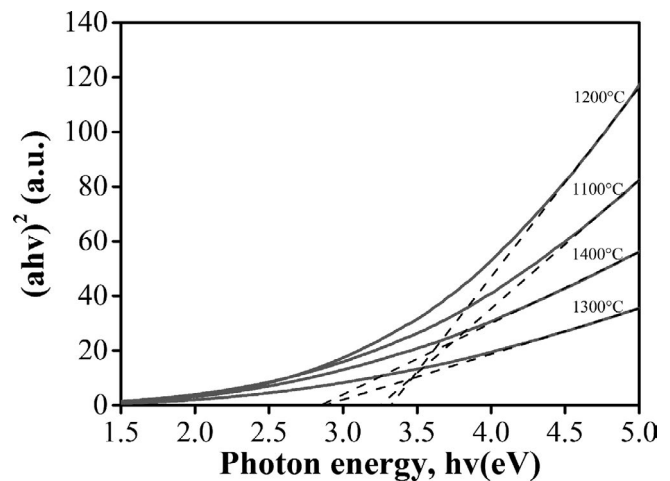| Pyrolysis temperature (°C)	$E_C - E_F$ (eV)	$E_A - E_F + w$ (eV)	T_0 (K)	σ_3 ($\Omega^{-1}cm^{-1}$)	χ_1^2
1100	0.69	0.36	4.93×10^7	1.42×10^0	0.07
1200	0.65	0.32	1.24×10^7	2.62×10^{-2}	0.06
1300	0.61	0.28	2.94×10^6	9.61×10^{-4}	0.01
1400	0.57	0.25	9.97×10^5	3.11×10^{-4}	0.01
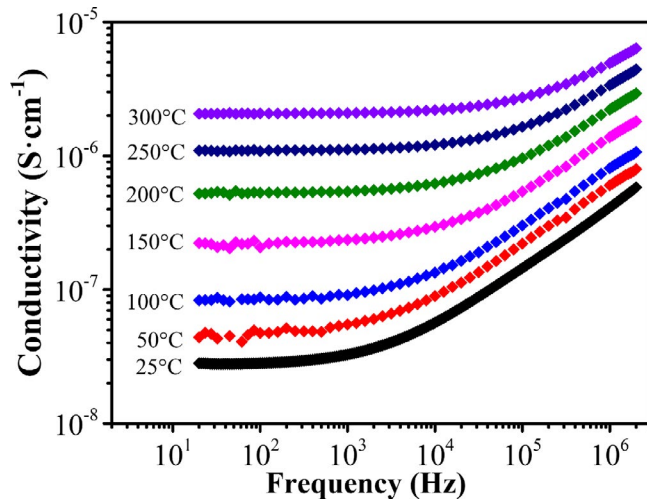
FIGURE 2 Effect of the frequency on the AC conductivity of amorphous silicoboron carbonitride pyrolyzed at 1200°C [Colour figure can be viewed at wileyonlinelibrary.com]

FIGURE 3 Bandgaps of samples pyrolyzed at different temperatures estimated by the *x*-intercept slope of the dashed line

transitions in the electronic structure with different n constants. For n = 1.5, Inkson and Pfost separately reported that E_T should represent the transition from a deep impurity trap to a delocalized band as follows [40,41]:

$$E_T = E_C - E_D \quad (5)$$

where E_C is the conduction band mobility edge and E_D is the defect level with a high density of state. To verify the effectiveness of the T_{auc} transition for a-SiBCN material, the low-energy range absorption behavior of the materials was determined and compared with the theoretical expression in Equation (4). The experimental and fitting data are showed in Figure 4 and Table 2. Good fittings were obtained with low χ_2^2 values, revealing the presence of Tauc transition in our materials. Besides, the fitting n constant was close to 1.5, such that the transition was produced between the deep defect states and the mobility edge.

As revealed by previous studies,[22,23,25] the dependency of the conductivity with the temperature in PDCs is associated with structural changes. To better understand the conduction behavior of the a-SiBCN ceramics, X-ray diffraction (XRD), nuclear magnetic resonance (NMR), and XPS measurements were conducted to characterize the structure of the materials. Figure 5A displays the XRD patterns of

TABLE 2 Fitting parameters for the optical absorption curves

Pyrolysis temperature (°C)	E_g (eV)	E_T (eV)	n	χ_2^2
1100	3.24	0.50	1.23	4.4×10^{-3}
1200	3.30	0.51	1.29	1.0×10^{-2}
1300	2.93	0.48	1.35	1.4×10^{-2}
1400	2.92	0.46	1.47	9.7×10^{-3}

SiBCN ceramics pyrolyzed at different temperatures. The pyrolyzed samples prepared herein showed no diffraction peaks and remained amorphous, with no noticeable crystalline features. In line with previous studies,[42] this phenomenon was produced by boron, which hindered crystallization.

The chemical bonds present were examined by NMR and XPS. Figure 5B shows the ^{29}Si NMR spectra of the a-SiBCN pyrolyzed at different temperatures. The spectrum could be deconvoluted into three peaks centered at −19, −34, and −50 ppm, corresponding to the reported chemical shifts of SiC_4, $SiCN_3$, and SiN_4 bonds, respectively.[4] Thus, the Si-based matrix presented three kinds of bonds, and their relative concentration can be calculated by the area of each peak (Table 3). Unlike SiN_4 and SiC_4, the concentration of
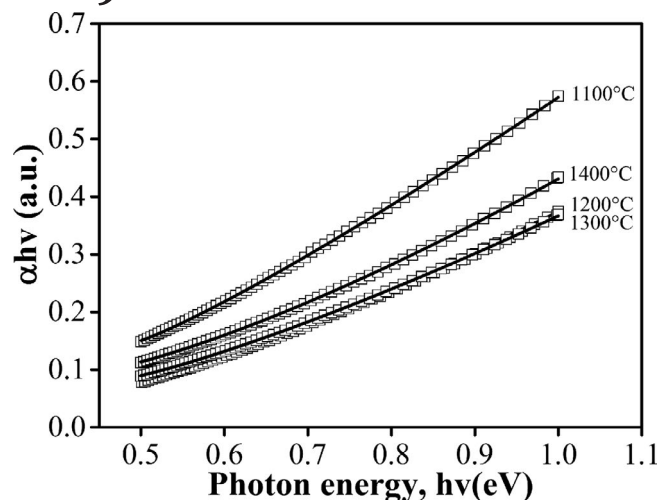
FIGURE 4 Experimental and fitting data for the low-energy range absorption behavior

SiCN$_3$ bonding units decreased with the pyrolysis temperature, revealing micro-scale structural separation processes in the Si matrix phase as the pyrolysis temperature increased.

TABLE 3 Mole percentage for the different silicon bonding environments, B–C and B–N bonds of amorphous silicoboron carbonitride ceramics

	1100°C	**1200°C**	**1300°C**	**1400°C**
SiCN$_3$	38.60%	30.86%	23.35%	17.88%
SiN$_4$	50.80%	55.72%	61.17%	65.19%
SiC$_4$	7.74%	9.87%	12.00%	13.69%
B-N	89.82%	91.94%	93.60%	95.57%
B-C-N	10.18%	8.06%	6.40%	4.43%

Figure 5C shows the B1s XPS spectra of the a-SiBCN ceramics. Curve-fitting of the spectrum revealed two peaks at 189.8 and 191 eV, corresponding to B–C–N, and B–N bonds, respectively.[44,45] The relative contents of both bonds are summarized in Table 3. The amount of B–N bonds was significantly higher than that of B–C–N bonds, suggesting that the B–C–N phase is mainly composed of BN$_3$ bonds. Besides, the amount of B–N bonds increased with the pyrolysis temperature, whereas the opposite trend was observed for B–C–N.
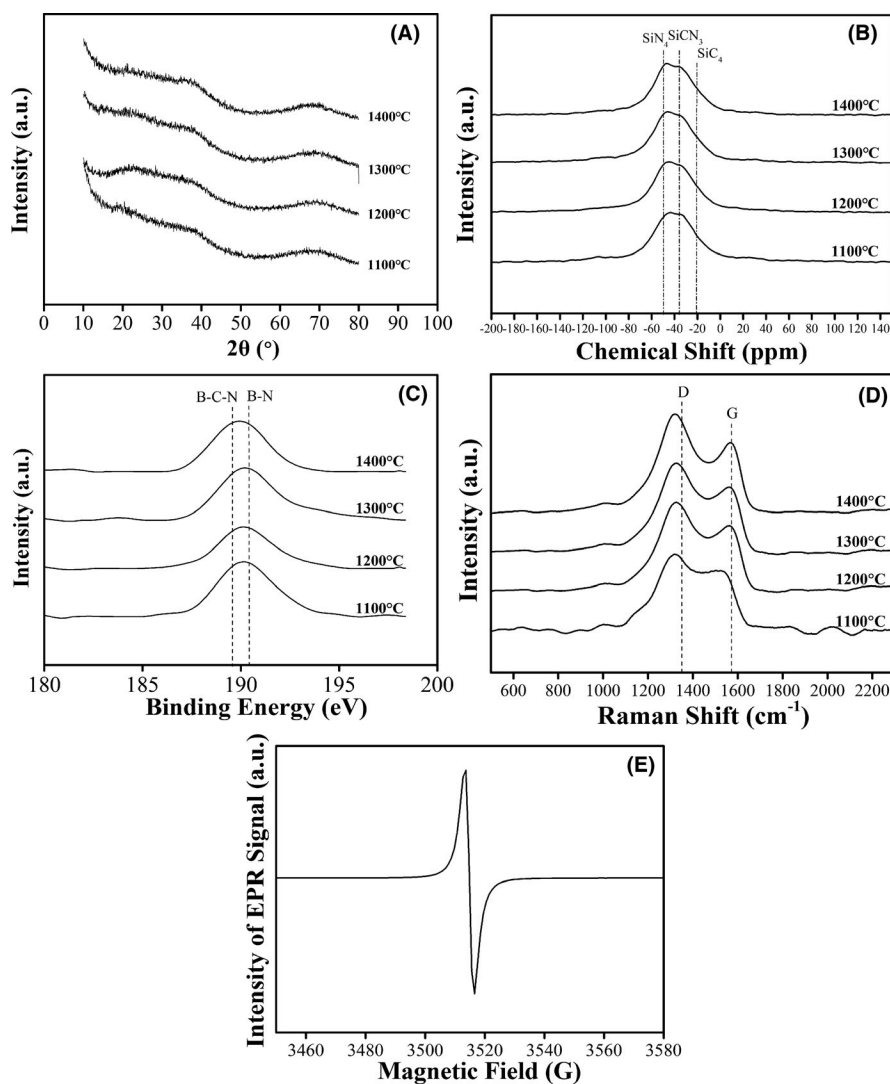

FIGURE 5 Structure analysis of the amorphous silicoboron carbonitride ceramics pyrolyzed at different temperatures: A, X-ray diffraction; B, ^{29}Si NMR; C, B1s XPS spectra; D, Raman spectroscopy; and E, typical electron paramagnetic resonance spectrum

The structural changes of the free carbon phase were further analyzed using Raman spectroscopy (Figure 5D). Two major bands were observed at 1350 and 1580 cm^{-1}, corresponding to the D and G bands of the free-carbon phase, respectively.[46] The presence of these two peaks indicated the presence of an amorphous carbon phase in our samples. The amount and type of point defects in the materials was studied by EPR. The typical spectrum of a sample pyrolyzed at 1200°C is shown in Figure 5E. The spectrum showed only one symmetric line with a g factor of 2.0032 ± 0.0002, confirming the presence of carbon-related dangling bonds (ie, unpaired electrons) in our materials.[47]

4 | DISCUSSION

4.1 | Hopping Mechanism

Previous investigations have revealed that the variation of conductivity with the testing temperature for PDCs materials reveals two different charge carrier transport behaviors at low temperatures. First, a 3D VRH reported by Haluschka et al and Hermann et al,[23,25] with opposite behaviors for the prefactor σ_3 and the characteristic temperature T_0 (Equation 1), as follow:

$$\sigma_3 \infty \left(T_0\right)^{-\frac{1}{2}} \quad (6)$$

This expression indicates that the conduction takes place within the defect energy level close to the Fermi level. Second, the BTH mechanism was investigated by Wang et al,[26] with the following relationship between T_0 and σ_3:

$$\ln \sigma_3 \infty \left(T_0\right)^{\frac{1}{4}} \quad (7)$$

This expression shows that electrons within the defect level fill empty states near the so-called "transport energy"

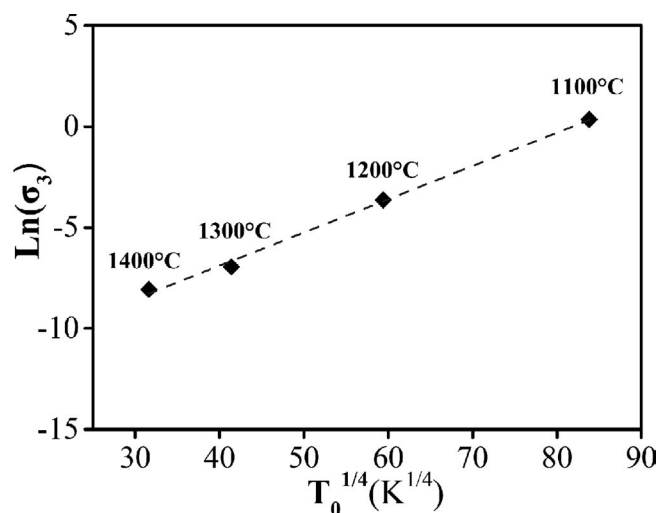(within band-tail) and then hop back to lower localized states. To determine the electrons transport mechanism prevailing in our materials, we represented T_0 vs σ_3 (Figure 6). A good linear relationship was obtained, suggesting that our materials followed the BTH conduction mechanism, rather than the previously assumed VRH mechanism.

We also analyzed the effect of an alternating electric field on the transport mechanism. The frequency-AC conductivity behavior at different testing temperatures could be separated in two regions namely, a low-frequency region and a high-frequency region. In the low-frequency region, conductivity shows a frequency-independent behavior. We used the conductivity measured at 20 Hz (σ_L) for the following analysis. The low-frequency conductivity as a function of the testing temperature can be calculated as follows:

$$\ln \sigma_L = -\left(\frac{T_1}{T}\right)^{\frac{1}{\beta}} + \ln \sigma_{L1} \quad (8)$$

where σ_{L1} is a constant, T_1 is the characteristic temperature, and β is a constant depending on the conduction mechanism. As shown in Table 4, the fitting parameter β is close to 4, which indicates that SiBCN ceramics followed the BTH conduction mechanism in the low-frequency region. In the high-frequency region, the conductivity showed a frequency-dependent behavior. The conduction mechanism was studied by determining the characteristic frequency (f_c), which is representative of the relaxation process and relates to the peak frequency in the frequency-imaginary part of the electric modulus relationship. f_c correlates with the testing temperature as follows:

$$\ln f_C = -\left(\frac{T_2}{T}\right)^{\frac{1}{\gamma}} + \ln f_0 \quad (9)$$

where f_0 and T_2 are constants. As shown in Table 4, the fitting parameter γ was close to 4, which indicated that the relaxation process in a-SiBCN ceramics remained controlled by the hopping process.

4.2 | Electronic structure

As revealed by the fitting results mentioned above, the a-SiBCN ceramics showed a BTH conduction mechanism, in line with previous reports on SiC and SiCN.[26,27] To explain the BTH mechanism in our materials, we considered the unique electronic structure of a-SiBCN, which was studied

FIGURE 6 Relationship between T_0 and σ_3

TABLE 4 Fitting parameters for the AC conductivity curves

Pyrolysis temperature (°C)	β	χ_3^2	γ	χ_4^2
1200	4.06	2.5×10^{-2}	4.02	1.4×10^{-1}
	0.98	2.7×10^{-1}	1.01	7.3×10^{-1}

by calculating the fitting data in Tables 1 and 2.[27] By combining these fitting results, we were able to schematically represent the obtained electronic structures (Figure 7). The change in these electronic structures and the relationship with the transport mechanism were discussed in terms of network structure changes as follows.

First, we focused on the bandgap information. The structure analysis results revealed that our material consisted of a Si-based matrix, a free carbon phase, and a B–C–N phase. The Si-based matrix contained an amorphous network comprised of SiC_4, $SiCN_3$, and SiN_4 units, while the B–C–N phase was mainly composed of BN_3 bonds. Owing to the non-transparency of free carbon, we hypothesized that the band gap of the a-SiBCN ceramics should be determined by the optic absorption of the Si-based and B-C-N phases. According to previous studies, the band gap of amorphous SiC, Si_3N_4, and BN_3 could vary between 2.0 and 5.0 eV, depending on the preparation process and the concentration.[48–50] The band gap value obtained herein (Figure 7) was within this range, thereby confirming our previous hypothesis. The bandgap shows decreased dramatically between 1200 and 1300°C. Based on a previous study on the electric structure of SiC, this sudden decrease in the bandgap could be related to significant hydrogen losses within this temperature range.[27]

Second, it is the existence of the defect level (E_D) and the band-tail band (E_A). The position of the defect level proved the existence of electronic defects in our materials. E_D is associated with carbon dangling bonds dispersed in the Si-based matrix. The presence of defects was also revealed by EPR (Figure 5E).

The band tail is associated with the disordered structure of materials. In our case, the band tail was produced by the amorphous structure of the Si-based and B–C–N phases, confirming the structure analysis information detailed above. Since the band-tail reveals deviations from periodic crystalline structure, we can obtain the degree of structural order of our materials by calculating the band-tail width between the ban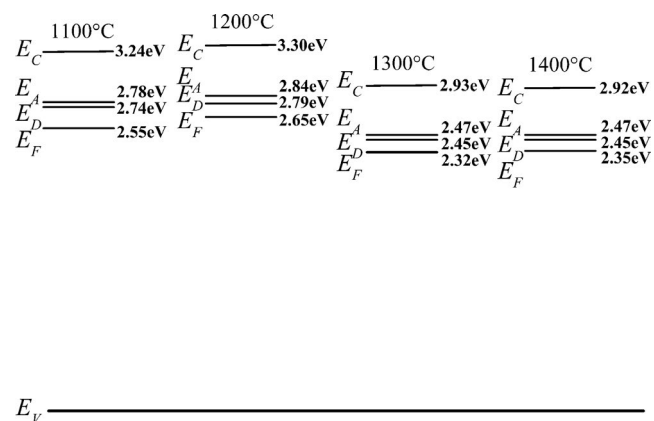d tail level and the edge of the conduction band. Thus, a reduction in the band-tail width is associated with a higher order in the structure. As shown in Figure 8, E_C-E_A changed slightly with the pyrolysis temperature. This stability of E_C-E_A suggested that structure ordering was hindered in a-SiBCN. These results were in line with the above structure analysis revealing that the disordered structure of SiBCN was preserved at these temperatures. Besides, SiBCN showed higher E_C-E_A values than other a-SiC ceramics (it changed from 0.40 to 0.16 eV upon increasing the temperature),[27] revealing a more disordered amorphous structure for the formers at similar pyrolysis temperatures. This can be attributed to the B–C–N phase, which hindered the rearrangement of the Si-based phase.

Third, and more interesting, it is the overlap between the band-tail and the defect level. This overlap provides the hopping conditions required for a BTH mechanism (ie, hopping tunnel for electrons to be transported from the defect level to near empty states, and subsequent hop back to band tail band). The explanation for this overlapping is two-fold. First, the unique polymer-to-ceramic preparation process led to the cleavage of chemical bonds and rearrangement processes, resulting in gas release and defects formation. Especially, the breaking of C–H bonds resulted in large amounts of carbon dangling bonds in our materials and, as a result, the high defect energy level in band gap. Second, the amorphous structure was maintained at high temperature, revealing the thermal stability of our materials. This amorphous network of the Si-based matrix and the inhibition effect of B–C–N phase resulted in significantly low atomic diffusion rates compared to crystalline Si-based ceramics. Thus, structure rearrangement and crystallization were hindered in our materials. As a result, the gap between the edge of the conduction band and band tail level is wide. Thus, the combining effect of the wide band-tail and the high defect energy level is likely responsible for the overlap.
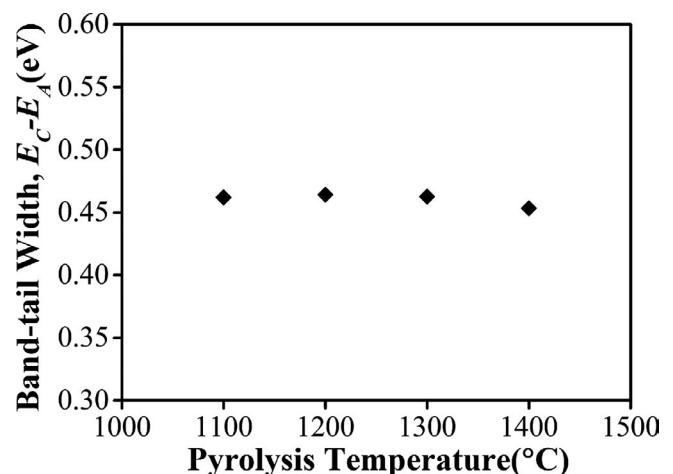

FIGURE 7 Schematic of the electronic structures

FIGURE 8 Band-tail width as a function of the pyrolysis temperature

Another interesting point is the different transport mechanisms of the a-SiBCN ceramics. Hermann et al reported that SiBCN ceramics followed VRH mechanism derived from their highly disordered structure and the presence of unsaturated bonds.[25] Despite having similar structure, our materials followed a BTH mechanism. We consider that this different mechanism could be related to different structure information used herein, which resulted in different gap distances between E_A, E_D, and E_F. As indicated above, a-SiBCN ceramics are rich in dangling bonds, thereby displacing E_F close to E_D. The formation of defect states within the band gap was produced by the existence of C-dangling bonds acting as electron donor defects. Consequently, an increase in the C-dangling bonds could lead to higher density of defect states, resulting in the Fermi level moving toward the conduction band, while we suppose the defect band would move slightly from the conduction band. Thus, the distance between the Fermi level and the defect band decreased. So, the hopping probability for electrons to move from E_D to E_F was higher compared to E_D to E_A, and electrons were transported following a VRH mechanism. In contrast, the electric structure of our materials (Figure 7) revealed lower E_A-E_D barriers compared to E_D-E_F, such that electrons would preferably hop from E_D to E_A rather than to E_F (ie, a BTH mechanism). Thus, we consider that the concentration of defects of the material is a very important factor determining the transport mechanism of SiBCN ceramics.

5 | CONCLUSIONS

The conduction mechanism of polymer-derived a-SiBCNs was investigated by measuring their temperature-dependent DC and AC conductivities, and the electronic structure was established by additional optical spectra measurements. The amorphous structure of the material was also studied by different techniques. The results revealed that the material contained three components: (a) a Si-based matrix, which consisted of SiC_4 tetrahedra, $SiCN_3$, and SiN_4; (b) a B–C–N phase, mainly composed of BN_3 with minor amounts of BCN_2; and (c) a free carbon phase consisting of amorphous carbon and C-dangling bonds. The materials maintained their amorphous structure upon increasing the pyrolysis temperature from 1100 to 1400°C.

The electric properties results showed that, regardless the pyrolysis temperature, all the samples exhibited band tail hopping under a DC/AC electric field. This hopping feature was explained by the unique electronic structure of the samples, with close band-tail and defect levels. This overlap was likely produced by the presence of a certain number of defects and the highly disordered structure of the materials. Unlike the VRH mechanism proposed in previous studies, we consider that the content of donor defects in our materials had a great influence on their electronic structure. The results also revealed that the electronic structure of the materials was affected by their structural evolution. The band-tail width of the material remained stable with the pyrolysis temperature, which was attributed to the stability of the amorphous network, favored by the inhibitory effect of the B–C–N phase.

ORCID

Kewei Wang [iD] https://orcid.org/0000-0002-4633-1804

REFERENCES

1. Schmidt WR, Narsavage-Heald DM, Jones DM, Marchetti PS, Raker D, Maciel GE. Poly(borosilazane) precursors to ceramic nanocomposites. Chem Mater. 1999;11:1455–64.

2. Weinmann M, Schuhmacher J, Kummer H, Prinz S, Peng J, Seifert HJ, et al. Synthesis and thermal behavior of novel Si–B–C–N ceramic precursors. Chem Mater. 2000;12:623–32.

3. Iwamoto Y, Völger W, Kroke E, Riedel R, Saitou T, Matsunaga K. Crystallization behavior of amorphous silicon carbonitride ceramics derived from organometallic precursors. J Am Ceram Soc. 2010;84:2170–8.

4. Seitz J, Bill J, Egger N, Aldinger F. Structural investigations of Si/C/N-ceramics from polysilazane precursors by nuclear magnetic resonance. J Eur Ceram Soc. 1996;16:885–91.

5. Haug J, Lamparter P, Weinmann M, Aldinger F. Diffraction study on the atomic structure and phase separation of amorphous ceramics in the Si−(B)−C−N system. 1. Si−C−N ceramics. Chem Mater. 2004;16:72–82.

6. Haug J, Lamparter P, Weinmann M, Aldinger F. Diffraction study on the atomic structure and phase separation of amorphous ceramics in the Si−(B)−C−N system. 2. Si−B−C−N ceramics. Chem Mater. 2004;16:83–92.

7. Widgeon S, Mera G, Gao Y, Stoyanov E, Sen S, Navrotsky A, et al. Nanostructure and energetics of carbon-rich SiCN ceramics derived from polysilylcarbodiimides: role of the nanodomain interfaces. Chem Mater. 2012;24:1181–91.

8. Chen Y, Yang X, Cao Y, Gan Z, An L. Quantitative study on structural evolutions and associated energetics in polysilazane-derived amorphous silicon carbonitride ceramics. Acta Mater. 2014;72:22–31.

9. Riedel R, Kienzle A, Dressler W, Ruwisch L, Bill J, Aldinger F. A silicoboron carbonitride ceramic stable to 2,000 degrees C. Nature. 1996;382:796–8.

10. Riedel R, Ruwisch LM, An L, Raj R. Amorphous silicoboron carbonitride ceramics with very high viscosity at temperatures above 1500°C. J Am Ceram Soc. 1998;81:3341–4.

11. Zhang L, Wang Y, Wei Y, Xu W, Fang D, Zhai L, et al. A silicon carbonitride ceramic with anomalously high piezoresistivity. J Am Ceram Soc. 2008;91:1346–9.

12. Wang Y, Zhang L, Xu W, Jiang T, Fan YI, Jiang D, et al. Effect of thermal initiator concentration on the electrical behavior of polymer-derived amorphous silicon carbonitrides. J Am Ceram Soc. 2008;91:3971–5.

13. Ryu H, Wang Q, Raj R. Ultrahigh-temperature semiconductor made from polymer-derived ceramics. J Am Ceram Soc. 2010;93:1668–76.

14. Wang K, Ma B, Wang Y, An L. Complex impedance spectra of polymer-derived silicon oxycarbides. J Am Ceram Soc. 2013;96:1363–5.

15. Ma B, Wang Y, Chen Y, Gao Y. Dielectric property and interfacial polarization of polymer-derived amorphous silicon carbonitride. Ceram Int. 2017;43:12209–12.

16. Yajima S, Hayashi J, Omori M. Continuous silicon carbide fiber of high tensile strength. Chem Lett. 1975;1975:931–4.

17. Colombo P, Paulson TE, Pantano CG. Synthesis of silicon carbide thin films with polycarbosilane (PCS). J Am Ceram Soc. 1997;80:2333–40.

18. Liu J, Zhang L, Hu F, Yang J, Cheng L, Wang Y. Polymer-derived yttrium silicate coatings on 2D C/SiC composites. J Eur Ceram Soc. 2013;33:433–9.

19. Li Y, Yu Y, San H, Wang Y, An L. Wireless passive polymer-derived SiCN ceramic sensor with integrated resonator/antenna. Appl Phys Lett. 2013;103:163505.

20. Liu Y, Liew L-A, Luo R, An L, Dunn ML, Bright VM, et al. Application of microforging to SiCN MEMS fabrication. Sens Act A. 2002;95:143-51.

21. Wang Y, Zhang L, Fan Y, Jiang D, An L. Stress dependent piezoresistivity in tunneling-percolation systems. J Mater Sci. 2009;44:2814-9.

22. Cordelair J, Greil P. Electrical conductivity measurements as a microprobe for structure transitions in polysiloxane derived Si–O–C ceramics. J Eur Ceram Soc. 2000;20:1947-57.

23. Haluschka C, Engel C, Riedel R. Silicon carbonitride ceramics derived from polysilazanes Part II. Investigation of electrical properties. J Eur Ceram Soc. 2000;20:1365-74.

24. Ionescu E, Francis A, Riedel R. Dispersion assessment and studies on AC percolative conductivity in polymer-derived Si–C–N/CNT ceramic nanocomposites. J Mater Sci. 2009;44:2055-62.

25. Hermann AM, Wang Y-T, Ramakrishnan PA, Balzar D, An L, Haluschka C, et al. Structure and electronic transport properties of Si–(B)–C–N ceramics. J Am Ceram Soc. 2001;84:2260-4.

26. Wang Y, Jiang T, Zhang L, An L. Electron transport in polymer derived amorphous silicon oxycarbonitrides ceramics. J Am Ceram Soc. 2009;92:1603-6.

27. Wang K, Li X, Ma B, Zhang M, Liu J, Wang Y, et al. Evolution in the electronic structure of polymer-derived amorphous silicon carbide. J Am Ceram Soc. 2015;98:2153-8.

28. Schwoerer-Böhning M, Macrander AT. Phonons in large-band-gap materials. J Phys Chem Solids. 2000;61:485-7.

29. Loong CK, Vashishta P, Kalia RK, Ebbsjö I. Crystal Structure and phonon density of states of high-temperature ceramic silicon nitride. Eur Phys Lett. 1995;31:201-6.

30. Hague JP. Gap modification of atomically thin boron nitride by phonon mediated interactions. Nanoscale Res Lett. 2012;7:303.

31. Shi X, Fu H, Shi JR, Cheah LK, Tay BK, Hui P. Electronic transport properties of nitrogen doped amorphous carbon films deposited by the filtered cathodic vacuum arc technique. J Phys: Condens Matter. 1998;10:9293-302.

32. Jonscher AK. The universal dielectric response. Nature. 1977;276:673-8.

33. Cheng C, Fan R, Wang Z, Xie P, Hou C, Fan G, et al. Radio-frequency negative permittivity in the graphene/silicon nitride composites prepared by spark plasma sintering. J Am Ceram Soc. 2018;101:1598-606.

34. Xie P, Zhang Z, Liu K, Qian L, Dang F, Liu Y, et al. C/SiO$_2$ meta-composite: Overcoming the λ/a relationship limitation in metamaterials. Carbon. 2017;125:1-8.

35. Qu Y, Du YU, Fan G, Xin J, Liu Y, Xie P, et al. Low-temperature sintering Graphene/CaCu3Ti4O12 nanocomposites with tunable negative permittivity. J Alloy Compd. 2019;771:699-710.

36. Al-Ani S, Higazy AA. Study of optical absorption edges in MgO-P$_2$O$_5$ glasses. J Mater Sci. 1991;26:3670-4.

37. Kshirsagar ST, Sinha A. Optical absorption, electrical conductivity and spectral response measurements on the system CdGaSSe. J Mater Sci. 1977;12:1614-24.

38. O'Connor P, Tauc J. Photoinduced midgap absorption in tetrahedrally bonded amorphous semiconductors. J Phys Rev B. 1982;25:2748-66.

39. O'Connor P, Tauc J. Spectrum of photoinduced optical absorption in a-Si:H. Solid State Commun. 1980;36:947-9.

40. Inkson JC. Deep impurities in semiconductors: II. The optical cross section. J Phys C: Solid State Phys. 1981;14:1093-101.

41. Pfost D, Liu H, Vardeny Z, Tauc J. Photoinduced absorption spectra in a-Ge: H and a-Si:H. Phys Rev B. 1984;30:1083-6.

42. Sarkar S, Gan Z, An L, Zhai L. Structural evolution of polymer-derived amorphous SiBCN ceramics at high temperature. J Phys Chem C. 2011;115:24993-5000.

43. Traßl S, Suttor D, Motz G, Rössler E, Ziegler G. Structural characterisation of silicon carbonitride ceramics derived from polymeric precursors. J Eur Ceram Soc. 2000;20:215-25.

44. Mannan MA, Noguchi H, Kida T, Nagano M, Hirao N, Baba Y. Chemical bonding states and local structures of the oriented hexagonal BCN films synthesized by microwave plasma CVD. Mat Sci Semicon Proc. 2008;11:100-5.

45. Mannan MA, Noguchi H, Kida T, Nagano M, Hirao N, Baba Y. Growth and characterization of stoichiometric BCN films on highly oriented pyrolytic graphite by radiofrequency plasma enhanced chemical vapor deposition. Thin Solid Films. 2010;518:4163-9.

46. Ferrari AC, Robertson J. Interpretation of raman spectra of disordered and amorphous carbon. Phys Rev B. 2000;61:14095-107.

47. Andronenko SI, Stiharu I, Misra SK. Synthesis and characterization of polyureasilazane derived SiCN ceramics. J Appl Phys. 2006;99:113907-11.

48. Kumbhar A, Patil SB, Kumar S, Lal R, Dusane RO. Photoluminescent, wide-bandgap a-SiC: H alloy films deposited

by cat-CVD using acetylene. Thin Solid Films. 2001;395:
244-8.

49. Deshpande SV, Gulari E, Brown SW, Rand SC. Optical properties
of silicon nitride films deposited by hot filament chemical vapor
deposition. J Appl Phys. 1995;77:6534-41.

50. Hoffman DM, Doll GL, Eklund PC. Optical properties of pyro-
lytic boron nitride in the energy range 0.05-10 eV. Phys Rev B.
1984;30:6051-6.